Polar Dyes in Solution: A Joint Experimental and Theoretical Study of Absorption and Emission Band Shapes

Barbara Boldrini, Enrico Cavalli, Anna Painelli,* and Francesca Terenziani

Dipartimento di Chimica GIAF, Università di Parma, INSTM-UdR Parma, I-43100 Parma, Italy

Received: January 9, 2002; In Final Form: April 15, 2002

Absorption and steady-state emission spectra of two fluorescent dyes are measured in a series of aprotic solvents with similar refractive index and different polarity. The spectra are interpreted in terms of a two-state electronic model accounting for the coupling to internal vibrations and to an effective solvation coordinate. The proposed approach naturally accounts not only for solvatochromic shifts of absorption and emission bands but also for the evolution of band shapes with solvent polarity and for the observation of nonspecular absorption and fluorescence bands. The good agreement between experimental and calculated spectra confirms the validity of a two-state picture for the low-energy spectral properties of these donor−acceptor molecules, provided that the molecular polarizability is fully accounted for. The role of conformational degrees of freedom in flexible chromophores is also addressed.

1. Introduction

Polar dyes are intensively studied as solvation probes;[1,2] the large solvatochromism that characterizes these molecules is in fact used to extract information on the complex phenomenon of solvation out of simple spectroscopic measurements in solution. The properties of the dyes themselves are however interesting. Largely fluorescent polar chromophores are common laser dyes and recently have been used as active molecules in tunable organic light-emitting diodes.[3] The first molecular rectifier belongs to this class of molecules,[4] which, generally, also show large nonlinear optical (NLO) responses and, specifically, are molecules of choice for second-order NLO applications.[5] Moreover, the intramolecular charge-transfer (CT) process occurring between the electron-rich (donor, D) molecular moiety and the electron-poor (acceptor, A) moiety, connected by a π-conjugated bridge, offers the opportunity to investigate the electron-transfer process.[6]

The analysis of the solvent-dependent absorption and emission frequencies of DA-conjugated chromophores yields information on the solvent polarity[1] or, conversely, can be used to get information on the solute properties.[7,8] This analysis is generally based on a fairly simple picture that describes the solvent as a continuum medium that reacts to the presence of a polar solute by generating a reaction field (F_R) proportional to the solute dipole moment (μ).[7] A good solvation probe is a molecule that linearly responds to the solvent perturbation, by lowering its energy by the amount μF_R, all other molecular properties being unaffected by solvation. This nonpolarizable solute hypothesis is the basis for the classical solvation theory, which predicts a linear dependence of absorption and emission frequencies on the solvent polarity.[7] This simple picture is, however, inadequate for highly polarizable DA-conjugated chromophores.[9] The failure of the classical solvation theory is most apparent in the large variation of absorption or emission band shapes or both with the solvent polarity,[10] but other effects, including solvatochromic effects in vibrational spectra[11,12] or time-dependent band shapes in time-resolved emission experiments,[13,14] point to the same direction.

Recently, we have developed a simple model for solvatochromism that preserves the simplicity of the classical solvation model but fully accounts for the molecular response to the reaction field at all orders.[10,11,15] Specifically, we describe the solvent as a continuum elastic medium that linearly responds to the presence of a polar solute. The solute is modeled in terms of two electronic states linearly coupled to molecular (internal) vibrations and to a solvation coordinate that describes orientational degrees of freedom of the surrounding solvent. Within this picture, we describe ground-state properties, including NLO responses,[15,16] and low-energy spectral properties, including steady-state and time-resolved electronic and vibrational spectra,[11,13,14] in terms of a few microscopic parameters that have to be extracted from the experiment. The model has been successfully applied to describe steady-state electronic and vibrational spectra of phenol blue,[12] an interesting nonfluorescent dye with large NLO responses[17] and with resonant Raman spectra[18] that show an anomalous dispersion with the excitation line. Here, we extend the analysis to two fluorescent dyes, DCM and nile red, the absorption and emission spectra of which are collected in several solvents, as described in section 2. On the basis of the model briefly summarized in section 3, we reproduce the observed spectra, addressing not only absorption and fluorescence frequencies but also band shapes and intensities, yielding to a complete spectroscopic characterization of these dyes (section 4). Nile red has a structure similar to phenol blue but with reduced flexibility due to the presence of an O-bridge that hinders the relative rotation of the groups attached to the central N atom (see Chart 1). The conformational flexibility of phenol blue is responsible for its nonluminescent behavior but also accounts for anomalous inhomogeneous broadening effects observed in its electronic and vibrational spectra.[12,18] In section 5, we compare absorption spectra of phenol blue and nile red dissolved in hexane, and on the basis of a simple extension of our model to describe conformational degrees of freedom, we relate the inhomogeneous broadening observed for phenol blue to its conformational flexibility. Section 6 summarizes and discusses main results.

* To whom correspondence should be addressed. Phone: +39-0521-905461. Fax: +39-0521-905556. E-mail: anna.painelli@unipr.it.

10.1021/jp020031b CCC: $22.00
Published on Web 06/07/2002

CHART 1

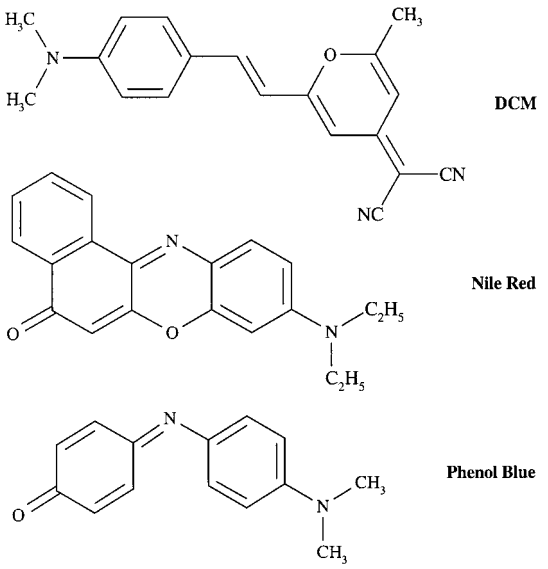

2. Experimental Methods and Results

The molecular structures of the chromophores studied in this work are shown in Chart 1. DCM [4-(dicyanomethylene)-2-methyl-6-(*p*-dimethylaminostyryl)-4*H*-pyran] is a commercial dye used as an efficient laser dye in the red. The molecule exhibits a broad and intense absorption band in the visible region that is related to the presence of two chromogenic groups linked by an unsaturated bridge: the dimethylamino electron-donor and the dicyanomethylene electron-acceptor group. Solutions of DCM prepared in the dark or in red light only contain the trans isomer,[19] but under room light, the solvated molecule undergoes photoisomerization to the cis form in a ratio that depends on the solvent and on the concentration of the solution.[19,20] The trans−cis isomerization barrier is high enough to prevent thermal isomerization for solutions kept in the dark. The absorption coefficient of the cis isomer is very low so that photoisomerization shows up in absorption spectra with a bleaching of the absorption band.[19] Photoexcitation of *cis*-DCM solutions does not produce any appreciable fluorescence.[19]

Nile red is a strongly fluorescent dye used for laser applications. An electron-donor diethylamino group is linked in nile red to a rigid structure that acts as an electron acceptor (see Chart 1). Nile red has found applications as a solvatochromic probe for pure solvents and solvent mixtures,[21] as well as to determine the micropolarity of polymers[22] or of Langmuir−Blodgett films of restricted geometries.[23] Phenol blue is a nonfluorescent dye with interesting second-order NLO responses.[17] It is characterized by D and A groups very similar to those of nile red, connected by the same π-conjugated bridge, apart from the lack of the O-bridge (see Chart 1).

DCM (Lambda Physics), nile red, and phenol blue (Aldrich) were purchased and used without further purification. Spectra- or HPLC-grade solvents, hexane, CCl_4, $CHCl_3$, CH_2Cl_2, and dimethyl sulfoxide (DMSO), were purchased from Aldrich. The choice of these solvents is due to the requirement of a large range of polarity, that is, of dielectric constant, in aprotic solvents with similar refractive index. As a matter of fact, the refractive index of hexane is lower than that of other solvents and, in this respect, the choice of cyclohexane as an apolar solvent would have been more appropriate. However, fluorescence spectra of both DCM and nile red evidenced aggregation problems in cyclohexane.

TABLE 1: Refractive Indexes (n_0) and Dielectric Constants (ϵ) of the Pure Solvents and the Frequencies of the Maxima of Absorption and Emission Bands Measured for DCM and Nile Red in the Different Solvents[a]

			DCM		nile red	
solvent	n_0	ϵ	ω_{abs}	ω_{em}	ω_{abs}	ω_{em}
hexane	1.375	1.89	22 000	18 900	20 550	19 050
CCl_4	1.460	2.24	21 700	18 350	20 000	18 200
$CHCl_3$	1.446	4.81	21 250	17 650	18 500	16 800
CH_2Cl_2	1.424	9.08	21 350	17 100	18 550	16 600
DMSO	1.478	46.7	20 900	15 600	18 100	15 800

[a] All frequencies are in cm^{-1}.

Electronic absorption spectra were measured with an ultraviolet−visible Jasco Uvidec 505 spectrophotometer. The Lambert−Beer law was verified in a concentration range from 10^{-5} to 10^{-6} M to exclude the possibility of autoaggregation or of other spurious effects. Fluorescence spectra have been measured on solutions of $\sim 10^{-6}$ M with a Spex-Fluorolog spectrometer, equipped with a xenon lamp. Excitation light wavelengths (in nanometers) for the different solutions were chosen as follows: 460 (CCl_4 and hexane), 470 ($CHCl_3$ and CH_2Cl_2), 480 (DMSO) for DCM; 490 (hexane), 500 (CCl_4), 540 ($CHCl_3$ and CH_2Cl_2), 550 (DMSO) for nile red. Fluorescence spectra collected on solutions with concentration ranging from 10^{-6} to 10^{-8} M were compared to verify the independence of spectral shape on concentration. The three dyes were easily dissolved in all solvents, except for DCM, which is poorly soluble in hexane. Solutions of DCM for absorption measurements were prepared under red light and stored in the dark.

The frequencies of the maxima of absorption and fluorescence bands for DCM and nile red dissolved in various solvents are reported in Table 1, together with the solvents' refractive indexes and dielectric constants. With increasing solvent polarity, both the absorption and the emission bands red-shift, the effect being more prominent for fluorescence. The oscillator strength is slightly affected by the solvent, smoothly increasing from 2.4 in CCl_4 to 2.6 in $CHCl_3$ and DMSO and to 2.7 in CH_2Cl_2 for DCM and from 0.9 in CCl_4, $CHCl_3$, and CH_2Cl_2 to 0.95 in DMSO for nile red. Fluorescence spectra, normalized to unit, and absorption spectra of DCM and nile red dissolved in hexane, $CHCl_3$, and DMSO are shown in Figure 1a,b and in Figure 2a,b, respectively. Spectra collected in other solvents are not shown for the sake of clarity but can be retrieved as Supporting Information. In nondipolar solvents (like hexane and CCl_4), the vibronic structure is fairly well-resolved in both absorption and fluorescence spectra. In polar solvents, the vibronic structure is completely smeared out. Absorption and fluorescence spectra are not specular; the relative intensities of the single vibronic transitions attest different Huang−Rys (HR) factors for absorption and emission processes. The red shift with increasing solvent polarity and the nonspecularity of absorption and fluorescence spectra are more pronounced for nile red than for DCM.

Absorption spectra of phenol blue dissolved in CCl_4, $CHCl_3$, and DMSO were already reported,[12] showing a red shift and an increase of oscillator strength with increasing solvent polarity. In section 5, we discuss the absorption spectrum of phenol blue dissolved in hexane.

3. The Model

DA-conjugated chromophores, also called push−pull chromophores, can be described as resonating between a fully neutral, $|DA\rangle$, and a zwitterionic, $|D^+A^-\rangle$, structure.[24] The

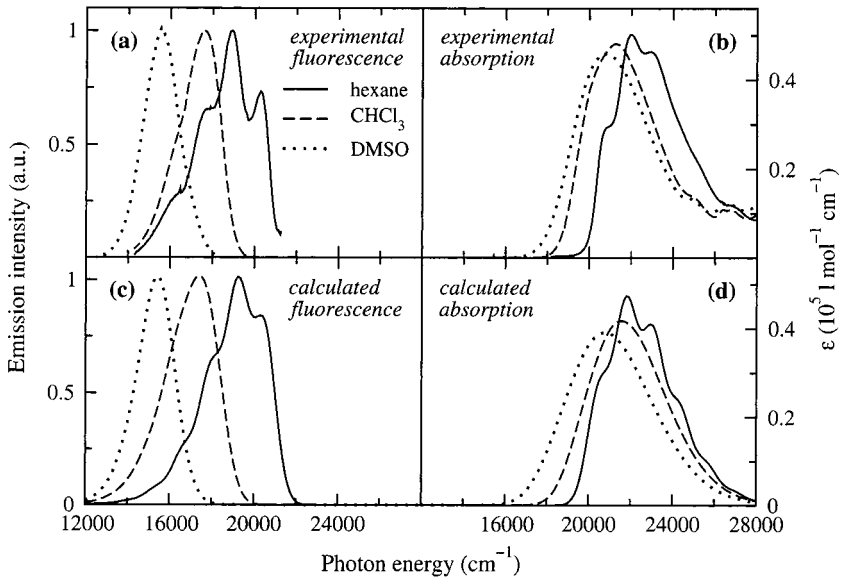

Figure 1. Experimental (a) fluorescence and (b) absorption spectra of DCM dissolved in hexane (continuous lines), $CHCl_3$ (dashed lines), and DMSO (dotted lines) and (c) fluorescence and (d) absorption spectra calculated according to the DCM parameters in Table 2 and for the ϵ_{or} in Table 3.

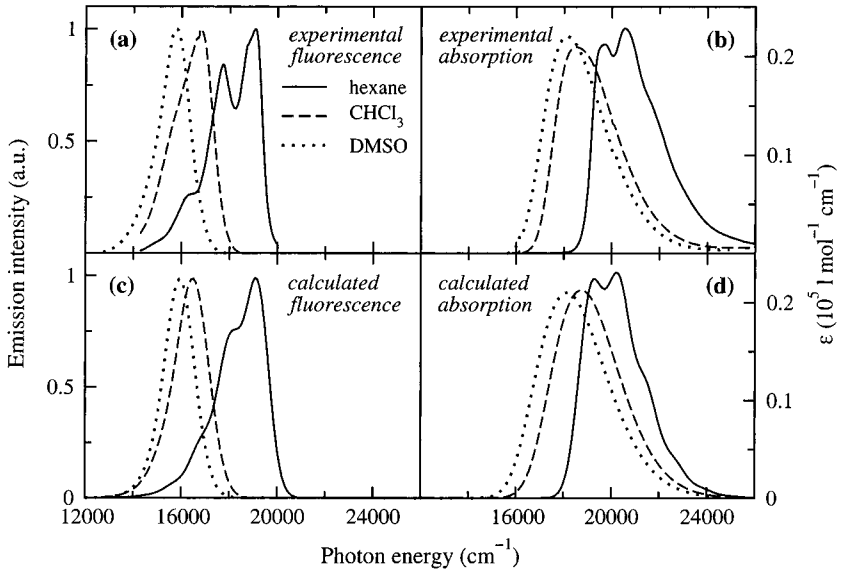

Figure 2. Experimental (a) fluorescence and (b) absorption spectra of nile red dissolved in hexane (continuous lines), $CHCl_3$ (dashed lines), and DMSO (dotted lines) and (c) fluorescence and (d) absorption spectra calculated according to the nile red parameters in Table 2 and for the ϵ_{or} values in Table 3.

resulting two-state Hamiltonian is defined by $2z_0$, the energy difference between the two states, and $-\sqrt{2}t$, the mixing matrix element. Within this picture, the ground state ($|G\rangle$) and the excited state ($|E\rangle$) are fully described by a single parameter, the ratio $z_0/\sqrt{2}t$.[25] This parameter fixes the degree of mixing between $|DA\rangle$ and $|D^+A^-\rangle$ states and, hence, the molecular polarity. We define the ionicity operator, $\hat{\rho}$, as counting electrons on the A site or, equivalently, as measuring the weight of $|D^+A^-\rangle$ in a given state. The ground-state ionicity, $\rho = \langle G|\hat{\rho}|G\rangle$ is a measure of the polarity of the molecule in the ground state, with $\rho = 0, 1$ for the pure $|DA\rangle$ and $|D^+A^-\rangle$ forms, respectively. The polarity of the excited state is $\langle E|\hat{\rho}|E\rangle = 1 - \rho$. The frequency and transition dipole moment for both absorption and emission processes are given by[16]

$$\hbar\omega_{abs/em} = \frac{\sqrt{2}t}{\sqrt{\rho(1-\rho)}}, \quad \mu_{abs/em} = \mu_0\sqrt{\rho(1-\rho)} \qquad (1)$$

where μ_0 is the dipole moment of $|D^+A^-\rangle$.

This simple model for the electronic structure can be extended to account for the coupling to molecular vibrations and for solvation effects. The coupling to internal vibrations is introduced in terms of few molecular normal coordinates (Q_i) with different equilibrium geometry but with the same frequency (ω_i) in $|DA\rangle$ and $|D^+A^-\rangle$ states.[16] This linear-coupling model, the so-called Holstein model, introduces for each coupled coordinate a parameter, ϵ_i, measuring the small-polaron binding energy, that is, the energy gained by $|D^+A^-\rangle$ because of the relaxation along Q_i. The total small-polaron binding energy is simply the sum of contributions from all coupled modes: $\epsilon_{sp} = \sum_i \epsilon_i$. We underline that ϵ_{sp} does not coincide with the standard definition of the vibrational relaxation energy: this last quantity in fact measures the relaxation energy gained by $|E\rangle$ after the $|G\rangle \rightarrow |E\rangle$ transition, while ϵ_{sp} refers to the $|DA\rangle \rightarrow |D^+A^-\rangle$ process so that the vibrational relaxation energy is, in general, a fraction of ϵ_{sp}.

To model solvation, we describe the solvent as a continuum

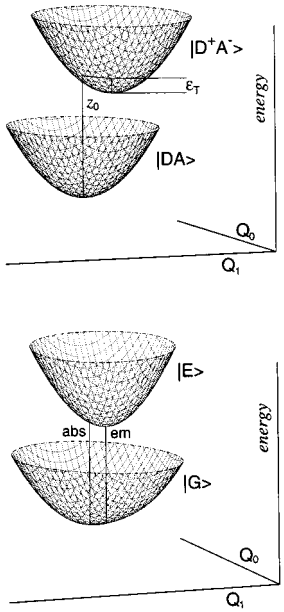

Figure 3. Potential energy surfaces calculated for the same parameters used below to fit spectra of DCM in DMSO. Parameters Q_0 and Q_1 describe the solvation and vibrational coordinate, respectively. The upper panel shows the harmonic potential energy surfaces for the two basis states ($\sqrt{2}t = 0$). The bottom panel shows the exact (anharmonic) potential energy surfaces for the ground and excited states of the interacting system ($\sqrt{2}t \neq 0$); abs and em label the vertical lines along which the absorption and emission processes occur. For the sake of clarity, in both panels, the energy gap between the two surfaces has been increased by a fixed amount.

dielectric medium linearly responding to the perturbation introduced by the polar solute.[15] This picture of course cannot describe site-specific solute−solvent interactions, such as H-bonds. Fast (electronic) degrees of freedom of the solvent can be renormalized out invoking the anti-adiabatic approximation.[15] In practice, these degrees of freedom need not to be introduced explicitly, their effect being accounted for by a renormalization of the model parameters, which become dependent on the solvent properties (mainly on the refractive index). The slow (orientational) degrees of freedom that characterize polar solvation are instead described by an overdamped solvation coordinate (Q_0) the equilibrium position of which is different in the two reference states. Q_0 then represents an additional Holstein coordinate the effective frequency, ω_0, of which is irrelevant to the subsequent discussion ($\hbar\omega_0 \ll kT$) and the small-polaron binding energy, ϵ_{or}, of which measures the relaxation energy of $|D^+A^-\rangle$ along Q_0. This solvation contribution adds to the small-polaron binding energy to give a total relaxation energy, $\epsilon_T = \epsilon_{sp} + \epsilon_{or}$.[15] The harmonic potential energy surfaces (PES) relevant to the two basis states are sketched in the upper panel of Figure 3 for a system with two coupled coordinates, Q_0 and Q_1.

Both internal (Q_i) and solvation (Q_0) coordinates can be treated within the adiabatic approximation. The adiabatic Hamiltonian is obtained by fixing all of the Q's to their equilibrium positions in either the ground or excited state.[15,16] The resulting Hamiltonian is the same two-state electronic Hamiltonian described above but with z_0 modified to account for the actual equilibrium geometry of the molecule and of the surrounding solvent. Because the equilibrium geometry is fixed by the electronic distribution itself, the adiabatic Hamiltonian describes a two-state system with z_0 substituted by a z parameter self-consistently depending on the ionicity: $z = z_0 - \epsilon_T\rho$ and $z = z_0 - \epsilon_T(1 - \rho)$ for the ground and excited state, respectively. Electronic and slow degrees of freedom (including molecular and solvation coordinates) are then connected in a feedback mechanism: the coupling of electrons to slow modes drives the electronic system toward a new electronic distribution (a new ρ) that in turn forces slow coordinates toward a new configuration in a typically nonlinear loop. This self-consistent mechanism amplifies static NLO susceptibilities of push−pull chromophores[15,16] and induces nonlinearity in all spectral responses of these molecules.[9] The nonlinearity of the system shows up clearly in the anharmonicity of the exact PES for the ground and excited states, drawn in Figure 3, lower panel.

Both absorption and fluorescence spectra involve vertical processes. The absorption process (see Figure 3, lower panel) occurs with slow coordinates frozen in the equilibrium configuration relevant to the ground-state polarity (ρ) and involves excitation toward the vertical excited state with ionicity $1 - \rho$. The corresponding transition frequency and dipole moment are again described by eq 1, with ρ measuring the ground-state polarity of the interacting system. After the vertical excitation, slow coordinates are no more in equilibrium and readjust in response to the different polarity of the excited state. The self-consistent interplay between electrons and slow coordinates implies that, during the relaxation along the excited-state PES, the electronic degrees of freedom also readjust following slow variables. As a consequence, the equilibrium ionicity in the excited state does not coincide with the vertical ionicity, $1 - \rho$, but assumes a different value that we define as $1 - \rho^*$.[10] The emission process (see Figure 3, lower panel) is then a vertical transition from a state at ionicity $1 - \rho^*$ toward the corresponding vertical ground state at ionicity ρ^*. The emission frequency and dipole moment are again given by eq 1 but with ρ replaced by ρ^*. Because absorption and emission processes involve different electronic states, that is, states with different polarity, there is not any immediate relation between absorption and emission band shapes, which are instead specular if a rigid picture for the electronic states is assumed. In other terms, the polarizability of the electronic system implies a variation of the electronic charge distribution during the relaxation of slow coordinates, leading to anharmonic PES (see Figure 3, lower panel)[9] and then justifying the observation of nonspecular absorption and emission band shapes.

In the framework of our model, the complex problem of relaxation of slow degrees of freedom after electronic excitation can be solved exactly to estimate the equilibrium polarity, $1 - \rho^*$, of the fully relaxed excited state from which fluorescence takes place.[10] In particular, we find $|1 - 2\rho^*| < |1 - 2\rho|$ so that, irrespective of having a neutral ($\rho < 0.5$) or an ionic ($\rho > 0.5$) chromophore, ρ^* is always nearer than ρ to the limiting 0.5 value (the cyanine limit). Molecular vibrations, with typical frequencies in the mid-infrared region, originate a vibronic structure in electronic spectra that, at the simplest level, can be described in a Franck−Condon picture. Within this approach, the HR factors for a system with just a single coupled molecular vibration are $\lambda_{abs} = (1 - 2\rho)^2\epsilon_{sp}/(\hbar\omega)$ and $\lambda_{em} = (1 - 2\rho^*)^2\epsilon_{sp}/(\hbar\omega)$ for absorption and emission, respectively; we always predict smaller HR factors for emission than for absorption spectra.[10] Moreover, HR factors are expected to decrease both in absorption and in emission as ρ moves toward 0.5 because in this limit the ground and excited state have exactly the same equilibrium geometry along all coupled modes. The slow, overdamped solvation coordinate is responsible for inhomogeneous broadening of electronic (and vibrational) spectra.[11] Once again inhomogeneous broadening effects are expected to vanish

TABLE 2: Molecular Parameters (eV) Fixed for the Two Dyes

parameter	DCM	nile red
$\sqrt{2}t$	0.88	0.95
z_0	1.14	0.88
ϵ_{sp}	0.45	0.33
ω	0.16	0.14

in the cyanine limit, where both absorption and emission spectra are described by a single sharp feature.

4. DCM and Nile Red Electronic Spectra

DCM and nile red both show positive solvatochromic behavior with absorption and emission bands moving to lower frequencies with increasing solvent polarity. On the basis of the standard theory of solvatochromism,[1] this suggests that the molecular dipole moment increases on excitation, that is, in our scheme, $\rho < 0.5$. Within the same standard picture, one can also easily rationalize the observation of much larger shifts in emission than in absorption spectra. More interesting is the fairly complex evolution of the band shapes with the solvent polarity. This phenomenon, not addressed by standard models for solvatochromism, offers useful information on the chromophore properties. For both DCM and nile red, spectra collected in apolar solvents, such as hexane, show a partially resolved vibronic structure, which is completely smeared out in polar solvents by inhomogeneous broadening effects. For both chromophores, the absorption band shape is, apart from inhomogeneous broadening, essentially unaffected by solvent polarity, with possibly a tiny narrowing of the absorption band of nile red in DMSO. Fluorescence spectra behave differently; they are not specular with respect to absorption spectra, and their shape changes considerably with the solvent polarity, suggesting a variation of the vibronic structure underlying the large spectral envelope with reduced HR factors in polar solvents. Because HR factors are proportional to $(1 - 2\rho)^2$ and $(1 - 2\rho^*)^2$ for absorption and emission spectra, respectively, this observation suggests that the excited state is much more sensitive to the environment polarity than the ground state.

To gain more information and to validate the proposed model, a fit of absorption and emission spectra is in order. On the basis of spectra collected in nondipolar solvents that show a partially resolved vibronic structure, we consider for both DCM and nile red a single coupled mode with frequency $\tilde{\nu}_v \approx 1300$ and ≈ 1100 cm^{-1}, respectively. To model absorption and emission spectra and their evolution with solvent polarity, three additional molecular parameters are needed: $\sqrt{2}t$, z_0, and ϵ_{sp}. Within our model, these parameters do not depend on the solvent polarity but vary with the solvent refractive index. Because the refractive indexes of the chosen solvents are similar (cf. Table 1), we neglect this dependence. With these parameters fixed, the solvent dependence of spectra is governed by a single additional parameter, ϵ_{or},[10,15] which depends on both solvent and solute properties but which, for each chromophore, is expected to increase with solvent polarity. The best fit of experimental data is obtained in terms of the molecular parameters listed in Table 2 and of the ϵ_{or} values in Table 3. Table 3 also lists calculated absorption and fluorescence frequencies. The comparison with experimental data in Table 1 is satisfactory, but we underline that the fitting procedure was aimed to reproduce not only frequencies but also band shapes. Figures 1 and 2 compare experimental and calculated spectra of DCM and nile red, respectively, for three different solvents: hexane as representative of apolar solvents, $CHCl_3$ as a medium-polarity solvent, and DMSO as a highly polar solvent. Fits of similar quality have been obtained for spectra collected in CCl_4 and CH_2Cl_2, which, for the sake of clarity, are not shown in the figures but are available as Supporting Information.

TABLE 3: Solvent Relaxation Energy, ϵ_{or} (eV), Estimated for the Two Dyes Dissolved in Different Solvents and Calculated Frequency Maxima (cm^{-1}) of the Absorption and Emission Bands

	DCM			nile red		
solvent	ϵ_{or}	ω_{abs}	ω_{em}	ϵ_{or}	ω_{abs}	ω_{em}
hexane	0	21 800	19 150	0	20 200	19 050
CCl_4	0.10	21 850	18 500	0.13	19 500	18 200
$CHCl_3$	0.32	21 500	17 500	0.47	18 700	16 500
CH_2Cl_2	0.35	21 450	17 200	0.50	18 600	16 400
DMSO	0.75	20 850	15 600	0.68	18 100	15 900

The spectra in Figures 1 and 2 are calculated by assigning each vibronic transition a Gaussian line-shape with standard deviation σ so that the molar absorption coefficient (ϵ) and the fluorescence intensity (I) are calculated as a function of the wavenumber ($\tilde{\nu}$) as follows:

$$\epsilon(\tilde{\nu}) = \frac{L\omega_{abs}\mu_{abs}^2}{60 \ln 10\, \hbar c^2 \epsilon_0} \frac{e^{-\lambda_{abs}}}{\sigma\sqrt{2\pi}} \sum_n \frac{\lambda_{abs}^n}{\sqrt{n!}} \times \exp\left\{-\left[\frac{\tilde{\nu}_{abs} - \lambda_{abs}\tilde{\nu}_v + n\tilde{\nu}_v - \tilde{\nu}}{\sqrt{2}\sigma}\right]^2\right\} \quad (2)$$

$$I(\tilde{\nu}) \propto \mu_{em}^2 \frac{e^{-\lambda_{em}}}{\sigma\sqrt{2\pi}} \sum_n \frac{\lambda_{em}^n}{\sqrt{n!}} \times \exp\left\{-\left[\frac{\tilde{\nu}_{em} + \lambda_{em}\tilde{\nu}_v - n\tilde{\nu}_v - \tilde{\nu}}{\sqrt{2}\sigma}\right]^2\right\} \quad (3)$$

where L is the Avogadro number, c is the speed of light, and ϵ_0 is the vacuum permittivity (in SI units). The index $n = 0, 1, 2, \ldots$ counts the vibronic levels separated by the vibrational frequency ($\tilde{\nu}_v$), and $\tilde{\nu}_{abs}$ and $\tilde{\nu}_{em}$ are the absorption and emission frequencies (from eq 1) in cm^{-1}. The choice of a Gaussian intrinsic line shape yields, in general, slightly better fits than a Lorentzian line shape, possibly indicating the presence of other sources of inhomogeneous broadening not explicitly accounted for in our model. However, we do not attach any specific physical meaning to the quite arbitrary choice of the intrinsic line shape, and σ is a fit parameter that we keep constant, irrespective of the solvent, just to minimize the number of adjustable parameters. The above equations are enough to describe spectra in apolar solvents ($\epsilon_{or} = 0$). In polar solvents, thermal disorder in the solvation coordinate locally affects the solute polarity so that the solution can be described in terms of a Boltzmann distribution of solute molecules with different polarity, each one in equilibrium with the local configuration of the surrounding solvent.[11] Absorption and emission spectra in polar solvents are then obtained by summing up the spectra calculated according to eqs 2 and 3 for molecules with different polarity, weighted by their Boltzmann probability.[11] All spectra in Figures 1 and 2 have been calculated with $\sigma = 510$ cm^{-1}, irrespective of the solvent. Despite this simple choice, the calculated spectra well reproduce inhomogeneous broadening in polar solvents, the nonspecularity of absorption and emission bands, and the strong evolution of fluorescence band shapes with the solvent polarity.

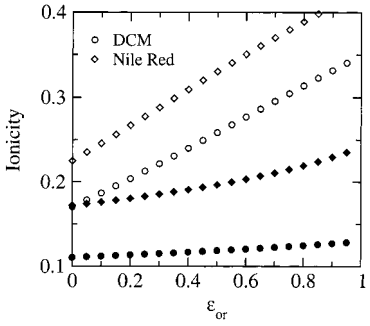

Figure 4. Ground-state ionicity as a function of ϵ_{or} ($\sqrt{2}t$ units) calculated for the parameters fixed for DCM (circles) and nile red (diamonds). Filled symbols refer to ρ; open symbols refer to ρ^*.

Overall, the agreement between calculated and experimental spectra is very good, particularly in view of the reduced set of parameters entering the fit. In this respect, we underline that μ_0, entering eq 2 via μ_{abs} (cf. eq 1) and then fixing the absolute value of $\epsilon(\tilde{\nu})$, is not a free parameter in the fit procedure, but its value is obtained from the measured oscillator strength, f, according to

$$f = \frac{2m_e\omega_{abs}}{e^2\hbar}\mu_0^2\rho(1-\rho) \tag{4}$$

where e and m_e are the electronic charge and mass, respectively. We estimate $\mu_0 = 28$ and 15 D for DCM and nile red, respectively. The negligible scattering of μ_0 values as obtained from oscillator strengths measured in different solvents, not exceeding 5% in either case, confirms the reliability of the proposed approach.

Having a simple physical picture for solvation, we can rationalize the observed behavior. Figure 4 reports the dependence of ρ (filled symbols) and ρ^* (open symbols) on ϵ_{or}, calculated on the basis of the fitting parameters in Table 1. DCM is an almost neutral molecule ($\rho \approx 0.12$ in apolar solvents). As a consequence, it is hardly polarizable, as demonstrated by the flat $\rho(\epsilon_{or})$ curve in Figure 4 (filled circles). As far as the absorption process is concerned, DCM is then a good approximation to the ideal nonpolarizable solvatochromic probe. The molecular polarizability however shows up in the emission process. First of all, after absorption, the excited-state ionicity readjusts following the relaxation of slow coordinates from the $1 - \rho$ value, relevant to the vertical state, to an appreciably different $1 - \rho^*$ value: absorption and emission band shapes are far from specular in any solvent. As a matter of fact, upon excitation the molecule feels a different effective electric field as originated by the interaction with slow degrees of freedom. Moreover, because the degree of mixing between $|DA\rangle$ and $|D^+A^-\rangle$ is larger in the excited state than in the ground state (i.e., $\rho^* > \rho$), the molecule in the excited state is more polarizable, and in fact, ρ^* increases with ϵ_{or} much faster than ρ (see Figure 4, open circles). Similar considerations hold for nile red, with the main difference that nile red is less neutral, its ground-state ionicity changing from $\rho \approx 0.17$ in hexane to $\rho \approx 0.20$ in DMSO (filled diamonds). Nile red is thus slightly more polarizable than DCM, as also demonstrated by the larger variation of absorption and emission band shapes with the solvent polarity.

5. Conformational degrees of freedom

Up to now, we have assumed that the charge-transfer integral, t, is not affected by the chromophore geometry. However, in flexible chromophores, torsional degrees of freedom are present that can modulate t, introducing a new kind of coupling.[26] Because conformational motions are very slow, they are expected to produce inhomogeneous broadening of optical spectra. In a previous paper,[12] to account for the unusual broadening of the absorption spectrum of phenol blue in CCl_4, a fairly large ϵ_{or} value for this solvent (almost twice as large as that for nile red) was fixed. Whereas finite ϵ_{or} for nondipolar solvents such as CCl_4 can be justified based on quadrupolar or octupolar (or higher order) interactions, we already suggested for phenol blue a possible role of conformational degrees of freedom.[12] To address this problem, we measured the absorption spectrum of phenol blue in hexane, a truly apolar solvent, in which multipolar solute−solvent interactions can be ruled out. The spectrum is shown in Figure 5a. In this spectrum the vibronic structure is completely smeared out, at variance with the spectrum of nile red in hexane (cf. Figure 2b). This difference can be ascribed to the conformational flexibility of phenol blue.

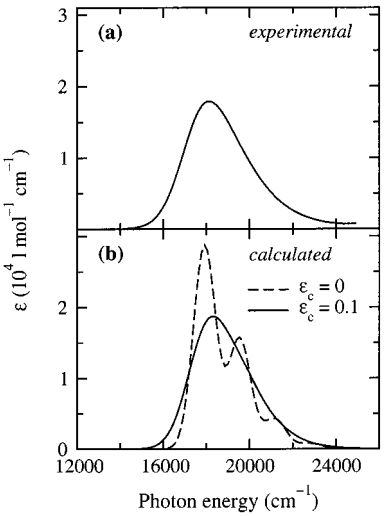

Figure 5. Experimental absorption spectrum (a) of phenol blue dissolved in hexane and (b) absorption spectrum calculated for $z_0 = 0.7$ eV, $\sqrt{2}t = 1.0$ eV at the equilibrium, $\epsilon_{sp} = 0.42$ eV, $\omega = 0.2$ eV, $\epsilon_{or} = 0$, and $\epsilon_c = 0$ (dashed line) and $\epsilon_c = 0.1$ eV (continuous line).

Conformational degrees of freedom modulate t, much as Peierls phonons in solid-state models. We define a reference conformation in which $t = t_0$. In the hypothesis of small deviations from this (otherwise arbitrary) conformation, a linear dependence of t on the conformational coordinate can be assumed so that it is convenient to define an effective conformational coordinate, Δ, measuring the deviation of t from the reference value: $t = t_0 + \Delta$. In the same hypothesis, a harmonic potential is associated to Δ with ϵ_c, the conformational relaxation energy, proportional to the inverse elastic constant for the conformational motion. On the basis of the two electronic states, $|DA\rangle$ and $|D^+A^-\rangle$, the Hamiltonian accounting for the coupling to a vibrational coordinate (Q) and to the conformational coordinate (Δ) reads

$$H = \frac{\Delta^2}{\epsilon_c} + \frac{1}{2}\omega^2Q^2 + \begin{pmatrix} 0 & -\sqrt{2}(t_0+\Delta) \\ -\sqrt{2}(t_0+\Delta) & 2z_0 - \sqrt{2\epsilon_{sp}}\omega Q \end{pmatrix} \tag{5}$$

Peierls coupling relevant to conformational degrees of freedom is qualitatively different from the Holstein coupling introduced for molecular vibrations or solvation coordinate. Holstein coupling in fact displaces the two reference PES relevant to $|DA\rangle$ and $|D^+A^-\rangle$ states along the coupled coordinates so that

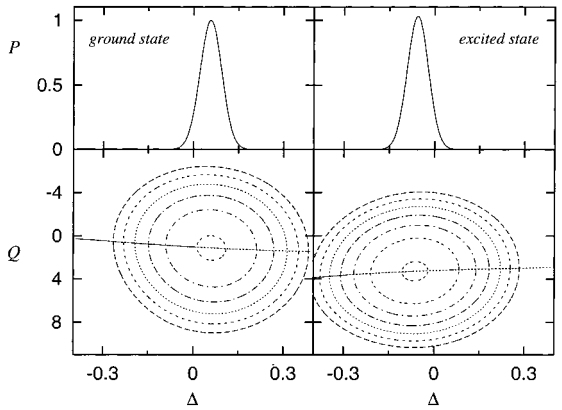

Figure 6. Isopotential lines (bottom panels) for the ground- and excited-state potential energy surfaces along the Q and Δ axes, in arbitrary units. The same parameters as in Figure 5 are used with $\epsilon_c = 0.1$ eV. The separation between potential levels is 0.2 eV. The almost straight lines are drawn across the equilibrium Q for each Δ. The upper panels show probability distributions of the Δ coordinate calculated along the equilibrium-Q lines in the lower panels.

the energy difference between the two reference states ($2z$) acquires a linear dependence on the Q's.[9] Conformational degrees of freedom do not displace the reference PES. Along the conformational coordinate, the two reference PES are exactly superimposed, and the energy difference between $|DA\rangle$ and $|D^+A^-\rangle$ does not depend on Δ. It is the matrix element that mixes the two reference states ($-\sqrt{2}t$) that linearly varies with the conformational coordinate and is therefore responsible for the variation of the amount of mixing of the two states with Δ.

Although different in nature, Holstein and Peierls couplings can be treated along the same lines. In the adiabatic approximation, Q and Δ are classical variables and the Hamiltonian in eq 5 can be diagonalized as a function of Q and Δ. Because of the Δ-dependence of the mixing matrix element in eq 5, for each Q, the two harmonic and superimposed PES relevant to the basis states are mixed to generate two anharmonic and displaced PES for the ground and excited state. In particular, with increasing Δ, the ground state is stabilized, whereas the excited state is destabilized so that the corresponding PES are displaced in opposite directions along Δ. In Figure 6, lower panels, we sketch the isopotential lines for the exact ground- and excited-state PES calculated as a function of Δ and Q. The two coordinates are not directly mixed in our model, but their interaction, mediated by the electronic system, shows up clearly in the tilt of the principal axes of the PES with respect to the Δ and Q axes. The tilt in fact indicates that in each one of the two states the equilibrium position for Q varies with Δ (or, conversely, the equilibrium position for Δ varies with Q). This is one more consequence of the molecular polarizability: any variation of either Δ or Q affects the electronic charge distribution driving the other coordinate into a new equilibrium.

The parameter Q represents a vibrational coordinate with typical frequencies in the mid-infrared so that at room temperature only the lowest vibrational state is occupied. The parameter Δ, corresponding to a slow conformational motion, is an overdamped coordinate with low characteristic frequency; as done for the solvation coordinate, we treat Δ as a classical coordinate and associate to it a Boltzmann distribution. The almost straight lines in the lower panels of Figure 6 are drawn across the equilibrium Q's for the ground and excited state, along which we calculate vertical absorption and emission spectra, respectively. Upper panels in the same figure report the probability distribution for the Δ coordinate calculated along this line for room temperature. Of course, the broad distribution of Δ is responsible for inhomogeneous broadening in the spectra of flexible molecules. Although the Δ distributions for the ground and excited state, shown in the upper panels of Figure 6, are similar, they correspond to regions with fairly different ionicity so that conformational broadening can affect in different ways absorption and emission spectra.

We are now in the position to discuss the absorption spectra of phenol blue in hexane. In Figure 5b, we report absorption spectra calculated with the same parameters adopted in ref 12, and fixing $\epsilon_{or} = 0$, for hexane, an apolar solvent. The dashed line corresponds to the spectrum calculated by imposing the same Gaussian width, $\sigma = 510$ cm^{-1}, as for nile red. The resulting spectrum is fairly well-resolved, and in this respect, it resembles the spectrum of nile red in hexane. The different band shape is related to the slightly larger ionicity of phenol blue[12] with respect to nile red, showing up with a smaller HR factor for phenol blue. This spectrum however does not bear any resemblance to the broad experimental spectrum in the upper panel, in which no vibronic structure can be recognized. As shown by the continuous line in Figure 5b, the experimental spectrum can instead be accurately reproduced on the basis of the same parameters (and the same $\sigma = 510$ cm^{-1}), provided that conformational disorder is accounted for, by introducing a small conformational relaxation energy, $\epsilon_c = 0.1$ eV.

6. Discussion and Conclusions

We have shown that absorption and steady-state emission spectra of DCM and nile red are well-described on the basis of two electronic states coupled to internal vibrations and to an effective solvation coordinate. The good agreement between experimental and calculated spectra in Figures 1 and 2 confirms the reliability of the model and of the chosen parameter set. The mesomeric dipole moment, an important quantity to estimate the static second-order NLO response, β, is an interesting by-product of our analysis. Two different mesomeric dipole moments can in general be defined: one accounting for the vertical excited state $\mu_m = \mu_0(1 - 2\rho)$ and the other one accounting for the relaxed excited state $\mu_m^* = \mu_0(1 - \rho - \rho^*)$. Of course, only the vertical excited state is relevant for the β estimate. We obtain $\mu_m \approx 22$ and 10 D for DCM and nile red, respectively, with no appreciable solvent dependence, according to the small polarizability of both dyes in the ground state, that is, to the small dependence of ρ on the solvent polarity. Standard estimates of mesomeric dipole moments from solvatochromism data[7] rely on steady-state emission frequencies and are then related to μ_m^*. For our chromophores, because of the appreciable polarizability of the relaxed excited state, μ_m^* weakly depends on solvent, varying with increasing solvent polarity from 20 to 15 D for DCM and from 9 to 6 D for nile red.

Our estimates for the mesomeric dipole moment of DCM and nile red compare favorably with literature data.[27,28] We underline however that our estimates of microscopic parameters, including the mesomeric dipole moment, do not require any information from microscopic models of solvation. In particular, the solvent is modeled as a continuum medium, linearly responding to the presence of a polar solute, but we do not need any assumption about the shape or the dimension of the cavity occupied by the solvent. The assumption of a spherical cavity, and, even worse, the need for an estimate of the cavity radius introduce instead very large and often uncontrolled uncertainties in the standard estimates of mesomeric dipole moments from solvatochromism data.[29] According to the standard procedure, the mesomeric dipole moment is estimated from the solvent

dependence of absorption and emission frequencies. Within our analysis, also intensities and band shapes are accounted for; enough information is extracted from experimental data to avoid any reference to other parameters from microscopic models.

The proposed model for spectral properties of DA chromophores in solution accounts for the solute polarizability and hyperpolarizabilities at all orders. Despite that, the number of independent parameters in the model is very small, at variance with a recently proposed approach that explicitly introduces the ground- and excited-state linear polarizabilities.[30] In fact, within the adopted two-state picture, the electronic polarizabilities and hyperpolarizabilities relevant to the ground and excited state of the chromophores are all fixed by the parameters of the electronic model (and, specifically, the ratio $z_0/\sqrt{2}t$ or, equivalently, ρ).[16] However, excited-state properties must be considered with care. In DA chromophores, the ground state interacts more strongly with the lowest-lying excited state (the one responsible for the absorption of visible light) than with higher excited states in the UV region. On this basis, the two-state model has been devised to describe the ground-state and low-energy spectroscopic properties. The excited state is, in this approach, an effective state, orthogonal to the ground state, that properly describes the CT transition but is not granted to bear any strict resemblance with any specific state of the real system. As is always the case for semiempirical models, the two-state model for DA chromophores has a well-defined applicability range: excited-state properties, such as dipole moment and (hyper)polarizabilities, are beyond its scope.

The model offers a simple yet reliable picture of the chromophore properties and is very useful to guide the synthesis of molecules with desired characteristics and to relate ground-state (hyper)polarizabilities to spectral features.[31] In this respect, we underline that the well-known and widely applied equation relating β to the absorption frequency and dipole moment and to the mesomeric dipole moment also relies on the two-state model. Therefore, the mesomeric dipole moment to be introduced in this equation is the difference between the dipole moment of the effective excited state within the two-state picture minus the ground-state dipole moment. Entering in this equation more refined estimates of the excited-state dipole moment, as obtained, for example, from quantum chemical calculations, is inconsistent and leads, in general, to unreliable results.

The same model described here has also been proposed by Hynes and co-workers to simulate static NLO responses of push−pull chromophores in solutions.[32,33] However the amplification of static NLO responses as originated from the self-consistent interaction between electronic and slow degrees of freedom (internal vibrations or polar solvation coordinate or both)[15,16,34] has not been recognized, and this is a possible origin of the inconsistencies between theoretical and experimental results on the dependence of static NLO responses on solvent polarity.[33]

The reliability of the two-state model to reproduce low-energy spectral properties of DA chromophores in solution is not granted a priori: its validity must be assessed from the comparison with experimental data. The evolution of absorption and emission bands with the solvent polarity is very well reproduced within our picture for both nile red and DCM. The variation of the emission band shape with the solvent polarity cannot be taken as a demonstration of the active role of other states beyond the first excited state or for the intervention of a special "twisting" coordinate connecting a vertical excited state to a twisted intramolecular CT state.[28,35] Of course, the relaxation of the excited state along a few coupled coordinates, either internal or external, plays a fundamental role in modifying the chromophore properties and then the shape of emission band. However, this is a very general phenomenon related to the chromophore polarizability and not to the presence of special coordinates.

The observation of different band shapes for absorption and steady-state emission spectra suggests quite naturally an evolution of the spectral band shapes in time-resolved emission experiments or, more generally, in experiments such as the pump−probe measurement, in which the temporal evolution of emission or absorption bands is observed. A preliminary discussion of these effects can be found in ref 13, but a more detailed analysis requires fairly sophisticated techniques to simulate the system dynamics along the coupled solvation and vibrational coordinates[14] and is beyond the scope of the present work. On the other hand, modeling time-resolved spectra requires estimates of the relaxation times of relevant degrees of freedom, including the longitudinal relaxation time of the solvent as well as the time scales for the vibrational and conformational relaxation. The steady-state spectra presented here, instead, do not rely on any specific choice of relaxation times. Relaxation dynamics does not affect steady-state spectra, in which only the characteristic frequencies are of concern. Vibrational frequencies are easily extracted from experimental data, whereas solvation and conformational frequencies are irrelevant provided that they are low enough to approximate the population of the corresponding energy levels in terms of Boltzmann distributions over a continuum of states.

In summary, we have reported absorption and fluorescence spectra of two fluorescent DA chromophores dissolved in a few solvents of different polarity. Subtle effects including the evolution of absorption and emission band shapes with the solvent polarity and the observation of nonspecular absorption and fluorescence bands are beyond standard approaches to solvatochromism but are naturally interpreted within models accounting for the solute polarizability and, specifically, for the nonlinear coupling between electronic degrees of freedom and slow modes (molecular vibrations and solvent degrees of freedom). Inhomogeneous broadening effects in polar solvents are another consequence of the solute polarizability, being reproduced in terms of a distribution of chromophore polarities. Another source of inhomogeneous broadening in optical spectra of flexible chromophores is recognized as conformational (torsional) degrees of freedom. These slow degrees of freedom are introduced in terms of an overdamped coordinate modulating the charge-transfer integral between D and A sites. Through this extension of the model, we have rationalized the different broadening observed in absorption spectra of nile red and phenol blue dissolved in nonpolar solvents.

Acknowledgment. We thank A. Girlando for useful discussions. Support from the Italian Ministry of University and Research (MIUR) and from the National Research Council (CNR) through "Progetto Finalizzato Materiali Speciali per Tecnologie Avanzate II" is gratefully acknowledged.

Supporting Information Available: Experimental and calculated spectra of DCM and nile red dissolved in CCl_4 and CH_2Cl_2 in Figures 1s and 2s. This material is available free of charge via the Internet at http://pubs.acs.org.

References and Notes

(1) Reichardt, C. *Chem. Rev.* **1994**, *94*, 2319.
(2) Fleming, G. R.; Cho, M. *Annu. Rev. Phys. Chem.* **1996**, *47*, 109.

(3) Bulović, V.; Shoustikov, A.; Baldo, M. A.; Bose, E.; Kozlov, V. G.; Thompson, M. E.; Forrest, S. R. *Chem. Phys. Lett.* **1998**, *287*, 455. Bulović, V.; Deshpande, R.; Thompson, M. E.; Forrest, S. R. *Chem. Phys. Lett.* **1999**, *308*, 317.

(4) Metzger, R. M.; Chen, B.; Höpfner, U.; Lakshmikantham, M. V.; Vuillaume, D.; Kawai, T.; Wu, X; Tachibana, H.; Hughes, T. V.; Sakurai, H.; Baldwin, J. W.; Hosch, C.; Cava, M. P.; Brehmer, L.; Ashwell, G. J. *J. Am. Chem. Soc.* **1997**, *119*, 10455.

(5) Kanis, D. R.; Ratner, M. A.; Marks, T. J. *Chem. Rev.* **1994**, *94*, 195.

(6) Myers Kelley, A. B. *J. Phys. Chem. A* **1999**, *103*, 6891.

(7) Liptay, W. *Angew. Chem.* **1969**, *8*, 177. Liptay, W. In *Excited States*; Lim, E. C., Ed.; Academic: New York, 1974; p 129.

(8) Horng, M. L.; Gardecki, J. A.; Papazyan, A.; Maroncelli, M. *J. Phys. Chem.* **1995**, *99*, 17311.

(9) Painelli, A.; Del Freo, L.; Terenziani, F. *Synth. Met.* **2001**, *121*, 1465.

(10) Painelli, A.; Terenziani, F. *Chem. Phys. Lett.* **1999**, *312*, 211.

(11) Painelli, A.; Terenziani, F. *J. Phys. Chem A* **2000**, *104*, 11041.

(12) Terenziani, F.; Painelli, A.; Comoretto, D. *J. Phys. Chem A* **2000**, *104*, 11049.

(13) Painelli, A.; Terenziani, F. *Synth. Met.* **2001**, *124*, 171.

(14) Terenziani, F.; Painelli, A. *Proc. Int. Sch. Phys.* "*Enrico Fermi*", in press.

(15) Painelli, A. *Chem. Phys.* **1999**, *245*, 183. Painelli, A. *Chem. Phys.* **2000**, *253*, 393.

(16) Painelli, A. *Chem. Phys. Lett.* **1998**, *285*, 352.

(17) Marder, S. R.; Beratan, D. N.; Cheng, L.-T. *Science* **1991**, *252*, 103.

(18) Yamaguchi, T.; Kimura, Y.; Hirota, N. *J. Chem. Phys.* **1998**, *109*, 9075.

(19) Drake, J. M.; Lesiecki, M. L.; Camaioni, D. M. *Chem. Phys. Lett.* **1985**, *113*, 530.

(20) Mialocq, J. C.; Armand, X.; Marguet, S. *J. Photochem. Photobiol. A* **1993**, *69*, 351.

(21) Deye, J. F.; Berger, T. A. *Anal. Chem.* **1990**, *62*, 615.

(22) Dutta, A. K.; Kamada, K.; Ohta, K. *J. Photochem. Photobiol. A* **1996**, *93*, 57.

(23) Dutta, A. K.; Kamada, K.; Ohta, K. *Chem. Phys. Lett.* **1996**, *258*, 369.

(24) Oudar, J. L.; Chemla, D. S. *J. Chem. Phys.* **1977**, *66*, 2664.

(25) Mulliken, R. S. *J. Am. Chem. Soc.* **1952**, *74*, 811.

(26) Toutounji, M. M.; Ratner, M. A. *J. Phys. Chem. A* **2000**, *104*, 8566.

(27) Meyer, M.; Mialocq, J. C. *Opt. Commun.* **1987**, *64*, 264.

(28) Ghoneim, N. *Spectrochim. Acta, Part A* **2000**, *56*, 1003.

(29) Lian, T.; Kholodenko, Y.; Hochstrasser, R. M. *J. Phys. Chem.* **1995**, *99*, 2546.

(30) Matyushov, D. M.; Newton, M. D. *J. Phys. Chem. A* **2001**, *105*, 8516.

(31) Marder, S. R.; Gorman, C. B.; Meyers, F.; Perry, J. W.; Bourhill, G.; Brédas, J.-L.; Pierce, B. M. *Science* **1994**, *265*, 632.

(32) Thompson, W. H.; Blanchard-Desce, M.; Hynes, J. T. *J. Phys. Chem. A* **1998**, *102*, 7712.

(33) Thompson, W. H.; Blanchard-Desce, M.; Alain, V.; Muller, J.; Fort, A.; Barzoukas, M.; Hynes, J. T. *J. Phys. Chem. A* **1999**, *103*, 3766.

(34) Del Freo, L.; Terenziani, F.; Painelli, A. *J. Chem. Phys.* **2002**, *116*, 755.

(35) Pommeret, S.; Gustavsson, T.; Naskreci, R.; Baldacchino, G.; Mialocq, J. C. *J. Mol. Liq.* **1995**, *64*, 101.